Self-Assembly of Symmetric Brush Diblock Copolymers

Weiyin Gu,[†] June Huh,[§,*] Sung Woo Hong,[†,⊥] Benjamin R. Sveinbjornsson,[‡] Cheolmin Park,[§] Robert Howard Grubbs,[‡,*] and Thomas P. Russell[†,*]

[†]Department of Polymer Science and Engineering, University of Massachusetts, 120 Governors Drive, Amherst, Massachusetts 01003, United States, [‡]Division of Chemistry and Chemical Engineering, California Institute of Technology, Pasadena, California 91125, United States, and [§]Department of Materials Science and Engineering, Yonsei University, 134 Shinchon-dong, Seodaemun-gu, Seoul 120-749, Korea. [⊥]Present address: Samsung Advanced Institute of Technology (SAIT), Mt. 14-1, Nongseo-dong, Giheung-gu, Yongin-si, Gyeonggi-do 446—712, Republic of Korea.

ABSTRACT Self-assembled structures of brush block copolymers (BrBCPs) with polylactide (PLA) and polystyrene (PS) side chains were studied. The polynorbornene-backbone-based BrBCPs containing approximately equal volume fractions of each block self-assembled into highly ordered lamellae with domain spacing ranging from 20 to 240 nm by varying molecular weight of the backbone in the bulk state, as revealed by small-angle X-ray scattering (SAXS). The domain size increased approximately linearly with backbone length, which indicated an extended conformation of the backbone in the ordered state. *In situ* SAXS measurements suggested that the BrBCPs self-assemble with an extremely fast manner which could be attributed to a reduced number of entanglements between chains. The strong segregation theory and Monte Carlo simulation also confirmed this near-linear dependence of the domain spacing on backbone length, rationalizing experimental results.

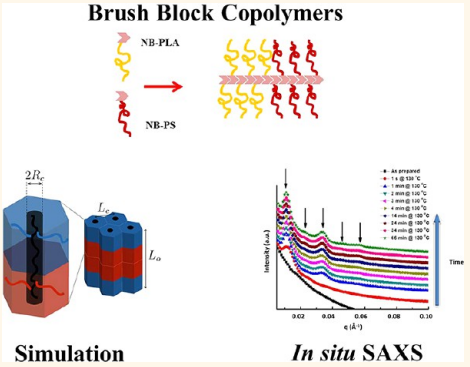

KEYWORDS: self-assembly · lamellae · brush block copolymer · fast kinetics · Monte Carlo simulation

Block copolymers (BCPs) have attracted tremendous interest from both academia and industry because of their ability to self-assemble into periodic structures with domain spacing ranging from 10 to 100 nm.[1,2] The incompatibility effects arising from the particular chemical structure of block copolymers give them a number of specific morphologies such as spheres, cylinders, lamellae, or gyroid, which leads to numerous technological applications.[3,4] For a noncrystalline A—B diblock copolymer, the bulk morphology is determined by Flory—Huggins parameter, χ, the total degree of polymerization, N, and volume fraction of each block, f. As the value of χN varies, three different regimes are distinguished: the weak (WSL), intermediate (ISR), and the strong (SSL) segregation limits. Notably, if $\chi N \gg 10$, the diblock copolymer is not only in SSL, where A and B blocks are strongly segregated, but it is also strongly stretched to create sharp microdomain interfaces. The characteristic domain spacing, D, is determined by the scaling relation of $D \sim N^{2/3}\chi^{1/6}$ in this region.[2,5]

Dedicated efforts have been made to tune the microphase separation distance by varying χ and N. In addition, macromolecular architecture is also a powerful tool for tuning BCP domain spacing. For example, Poelma *et al.* recently found that thin film self-assembly of cyclic polystyrene-*block*-polyethylene oxide (cPS-*b*-PEO) showed significant decrease in domain spacing over the corresponding linear polymers due to the reduced hydrodynamic radii of the cyclic systems.[23] Although small microstructure sizes are of particular interest,[6,7] especially to semiconductor industries, such as for storage media fabrication and lithographic applications,[24,25] it remains a challenge to obtain BCPs that self-assemble into morphologies with domain sizes exceeding 100 nm. Materials with large domain sizes have exciting applications as optical materials, such as polarizers and photonic band gap materials for visible and infrared light.[8,9,22] It is noted that, according to the model system for polymers with molecular weight (MW) over the critical entanglement MW, the viscosity of polymers increases abruptly as the MW gets larger due to severe chain entanglements, resulting in significant reduction of polymer mobility. Consequently, there could be a

* Address correspondence to russell@mail.pse.umass.edu, rhg@caltech.edu, junehuh@yonsei.ac.kr.

Received for review December 19, 2012 and accepted January 31, 2013.

Published online January 31, 2013
10.1021/nn305867d

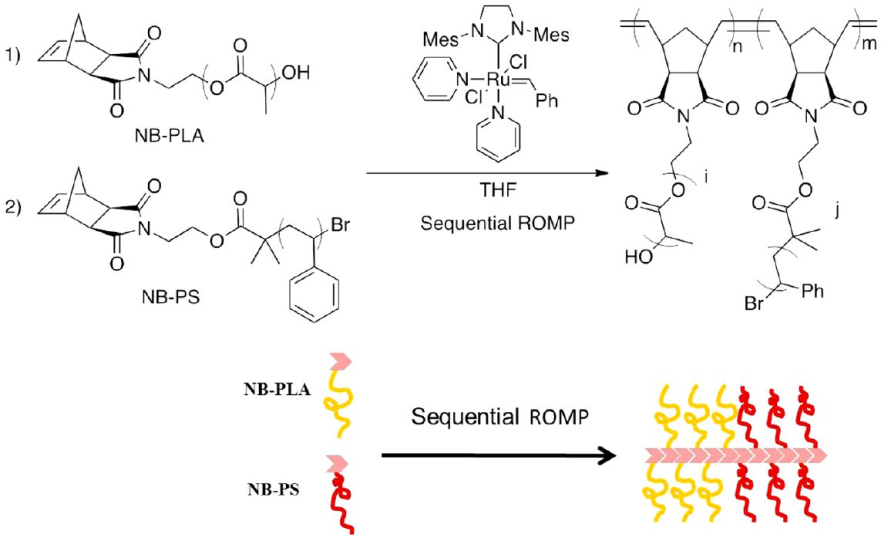

Scheme 1. General synthetic route and schematic diagram of BrBCPs.

serious degradation of polymer chains due to significantly increased annealing temperatures and time for molecular arrangement, and the defects might not be effectively annihilated due to the severe entanglements.[1,2,5,10]

Brush block copolymers (BrBCPs) where two or more different types of side chains are attached to a linear polymer in a block-wise manner may open up an alternative approach to obtain domain spacing with a broader range of length scales. In that case, each side chain may be designed long enough to drive microphase separation and thus behave like a block segment in a conventional block copolymer. Moreover, brush polymers have been considered to have the highly extended backbone conformation and exhibit the reduced degree of entanglements between brush polymers compared with conventional polymers, due to the significant steric hindrances between densely grafted side brush chains. Runge *et al.* found that high MW BrBCPs can self-assemble into exceptionally large structures with domain spacing exceeding 100 nm in the bulk state.[11] More recently, Xia *et al.* reported highly ordered lamellae structures with bulk domain spacing as large as 116 nm from the self-assembly of high MW, narrowly dispersed BrBCPs.[12] In their report, they concluded that the domain size was dictated by the backbone length but did not provide quantitative molecular weight dependence of backbone and side chain on the domain spacing, which is one of the essential guidelines for the tuning of microstructure formed by BrBCPs.

Here, we use a series of well-defined BrBCPs, which have similar chemical structures to the previously reported ones, to study their self-assembly behavior in the bulk state. The general synthetic route and schematic diagram of those BrBCPs are shown in Scheme 1. More specifically, ω-norbornenyl macromonomers containing polystyrene (NB-PS) and polylactide (NB-PLA) were prepared by sequential ring-opening metathesis polymerization (ROMP) according to the reported procedure (Gel permeation chromatography (GPC) data can be found in Supporting Information, Figure S1).[12,22] The MW of brush side chain and degree of polymerization of each block were intentionally controlled to be symmetric. Table 1 summarizes two sets of samples ($[g\text{-}S_x]_p\text{-}b\text{-}[g\text{-}LA_y]_q$) used, and the sample codes and characteristics of BrBCPs are clearly described there. Note that the subscripts x and y represent the molecular weight of side chains of each type (S represents NB-PS and LA represents NB-PLA), and subscripts p and q represent the number of the side chains. Small-angle X-ray scattering (SAXS) experiments were used to determine the bulk morphology, and the kinetic self-assembly process was also studied by performing an *in situ* SAXS experiment. The strong segregation theory and Monte Carlo simulation are in good agreement with those experimental results. Both

TABLE 1. Sample Codes and Characteristics of BrBCPs

group	sample codes	Mn[a] (kDa)	polydispersity index (PDI)	total degree of polymerization (DP)[a]
I	$[g\text{-}S_{2.4k}]_{19}\text{-}b\text{-}[g\text{-}LA_{2.4k}]_{25}$	105	1.01	44
	$[g\text{-}S_{2.4k}]_{35}\text{-}b\text{-}[g\text{-}LA_{2.4k}]_{43}$	186	1.01	78
	$[g\text{-}S_{2.4k}]_{51}\text{-}b\text{-}[g\text{-}LA_{2.4k}]_{67}$	281	1.03	118
	$[g\text{-}S_{2.4k}]_{98}\text{-}b\text{-}[g\text{-}LA_{2.4k}]_{124}$	529	1.08	222
	$[g\text{-}S_{2.4k}]_{189}\text{-}b\text{-}[g\text{-}LA_{2.4k}]_{233}$	1007	1.24	422
	$[g\text{-}S_{2.4k}]_{259}\text{-}b\text{-}[g\text{-}LA_{2.4k}]_{381}$	1525	1.61	640
II	$[g\text{-}S_{4.3k}]_{11}\text{-}b\text{-}[g\text{-}LA_{4.5k}]_{14}$	104	1.01	25
	$[g\text{-}S_{4.3k}]_{19}\text{-}b\text{-}[g\text{-}LA_{4.5k}]_{25}$	192	1.01	44
	$[g\text{-}S_{4.3k}]_{32}\text{-}b\text{-}[g\text{-}LA_{4.5k}]_{42}$	320	1.02	74
	$[g\text{-}S_{4.3k}]_{42}\text{-}b\text{-}[g\text{-}LA_{4.5k}]_{58}$	432	1.03	100
	$[g\text{-}S_{4.3k}]_{93}\text{-}b\text{-}[g\text{-}LA_{4.5k}]_{128}$	954	1.04	221
	$[g\text{-}S_{4.3k}]_{206}\text{-}b\text{-}[g\text{-}LA_{4.5k}]_{278}$	2089	1.13	484

[a] Determined by THF GPC using RI and MALLS detectors.

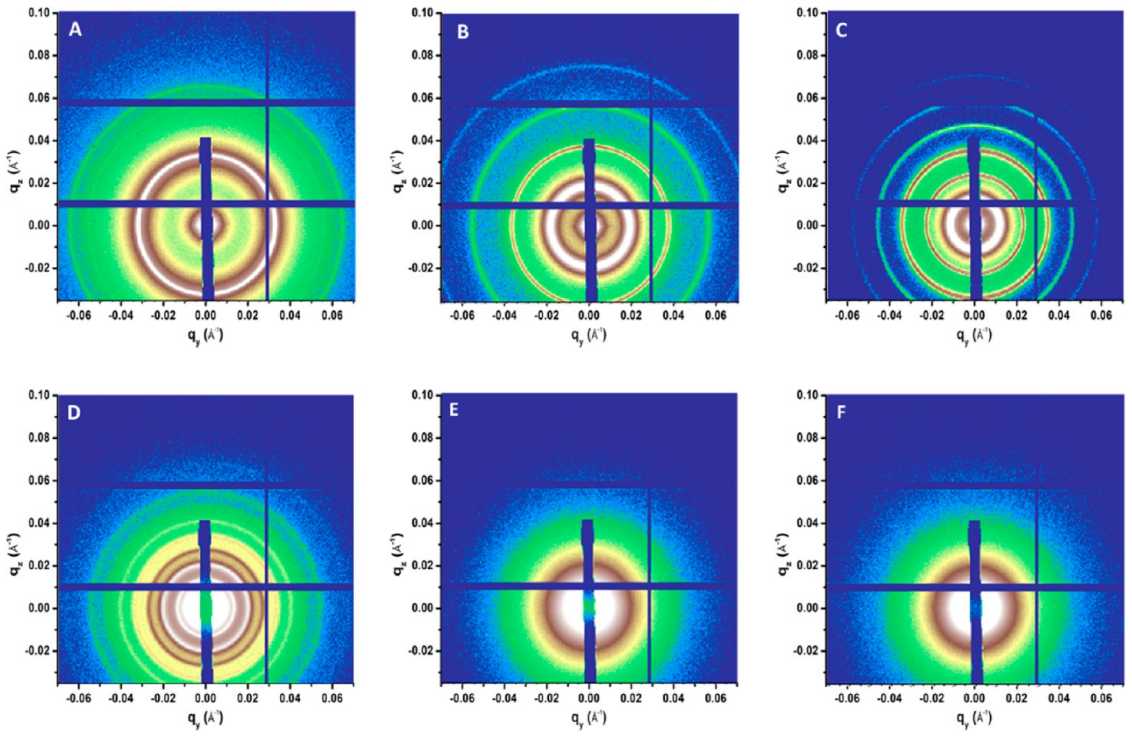

Figure 1. Representative 2D SAXS patterns for (A) [*g*-$S_{2.4k}$]$_{19}$-*b*-[*g*-$LA_{2.4k}$]$_{25}$; (B) [*g*-$S_{2.4k}$]$_{35}$-*b*-[*g*-$LA_{2.4k}$]$_{43}$; (C) [*g*-$S_{2.4k}$]$_{51}$-*b*-[*g*-$LA_{2.4k}$]$_{67}$; (D) [*g*-$S_{2.4k}$]$_{98}$-*b*-[*g*-$LA_{2.4k}$]$_{124}$; (E) [*g*-$S_{2.4k}$]$_{189}$-*b*-[*g*-$LA_{2.4k}$]$_{233}$; and (F) [*g*-$S_{2.4k}$]$_{259}$-*b*-[*g*-$LA_{2.4k}$]$_{381}$.

experiments and computational results show that domain spacing increases approximately linearly with the degree of polymerization of the backbone, suggesting an extended conformation of the backbone.

RESULTS AND DISCUSSION

Self-Assembly of BrBCPs in Bulk. Bulk samples were prepared in aluminum washers which were sandwiched by Kapton films and kept in a vacuum oven for 12 h or longer to achieve thermal equilibrium before SAXS measurements were taken (for details, see Experimental SAXS section). Circular patterns were observed in the 2D SAXS results from bulk samples of group I and group II (Figure 1 and Figure 2). Samples with low MW in each series showed distinguishable multiple ring patterns (Figure 1A−D and Figure 2A−E), indicating that well-ordered microphase structures were formed isotropically in the bulk state. Meanwhile, the domain spacing of high MW samples (Figure 1E, 1F and Figure 2F) may have been too large and beyond the limit of SAXS or microdomains may not have been as well-ordered. Profiles of the scattering intensity *versus* scattering vector were also generated from Figure 1 and Figure 2 and are shown in Figure 3A, and 3B, respectively. A systematic decrease in q^*, the scattering vector of the first-order reflection, was observed from low MW BrBCP to high MW BrBCP, indicating the anticipated increase of the domain spacing, ranging from 19.2 to 235 nm (Table 2). Strong reflections were also seen at integral multiples of q^* in most cases, indicating the lamellar nature of the microdomains with long-range lateral ordering, as expected due to the near symmetric volume fractions of the PS and PLA segments.

To analyze the relationship between the measured domain spacing, L_o, and DP of the backbone further, L_o was plotted against total degree of polymerization, DP, in the log−log plot (Figure 4). The exponents ν in the scaling form $L_o \sim DP^{\nu}$ for both cases were determined from the slope: $\nu = 0.84$ for group I and $\nu = 0.91$ for group II. Both values are greater than the power law index determined in the SSL region, which is 2/3, and they were also even greater than the greatest value previously reported, to the best of our knowledge, for a polystyrene-*block*-polylactide (PS-*b*-PLA)-based BCP system (0.81).[13,14] This suggests that the backbones of BrBCPs are highly stretched as the PS and PLA side chains are segregated from each other since the stretching of the backbone decreases the PS/PLA interfacial area per unit volume. Since group II BrBCPs have longer side chains compared with group I, steric hindrance may make the backbone more rigid and, thus, cause the ν value to be even larger.

In order to analyze this scaling relation that must be strongly related to the molecular packing of BrBCPs into a lamellar phase, we also simulated a model system of a molten BrBCP by the Metropolis Monte Carlo method with the 8-site bond fluctuation model.[15,16] The detailed description of the simulation method and parameters are given in Simulations section.

The morphologies of BrBCPs were simulated with various combinations of parameters (*N*,*M*) where the

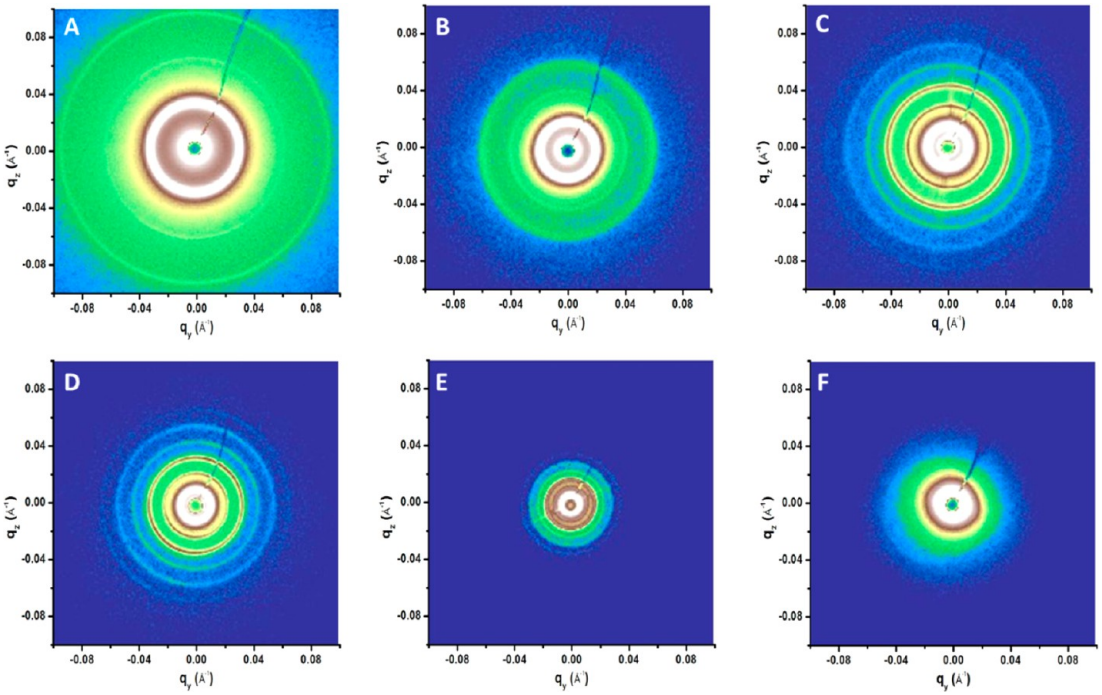

Figure 2. Representative 2D SAXS patterns for (A) $[g\text{-}S_{4.3k}]_{11}$-b-$[g\text{-}LA_{4.5k}]_{14}$; (B) $[g\text{-}S_{4.3k}]_{19}$-b-$[g\text{-}LA_{4.5k}]_{25}$; (C) $[g\text{-}S_{4.3k}]_{32}$-b-$[g\text{-}LA_{4.5k}]_{42}$; (D) $[g\text{-}S_{4.3k}]_{42}$-b-$[g\text{-}LA_{4.5k}]_{58}$; (E) $[g\text{-}S_{4.3k}]_{93}$-b-$[g\text{-}LA_{4.5k}]_{128}$; and (F) $[g\text{-}S_{4.3k}]_{206}$-$b$-$[g\text{-}LA_{4.5k}]_{278}$.

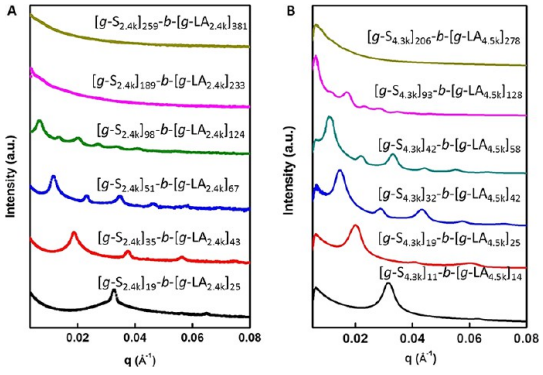

Figure 3. One-dimensional SAXS profiles calculated from the 2-D SAXS patterns in Figure 1 and Figure 2, respectively. (A) Group I. (B) Group II. Profile curves were offset for clarity.

backbone length N and the length of side chain M vary from $N = 6$ to $N = 30$ and from $M = 3$ to $M = 12$, respectively (Figure 5A). For comparison, the case of $N = 0$, which corresponds to symmetric diblock copolymer with chain length $2M$, was also simulated. The morphologies show that the system undergoes transition from disordered to lamellar phase by increasing either N or M, as summarized in the phase map shown in Figure 5B. A large reduction of translational entropy of A and B side chains attached to the backbone leads to the promotion of the phase separation when compared to the AB diblock case ($N = 0$).

The detailed molecular packing of BrBCPs into the lamellar phase was examined by the density profiles of the system components across the lamellar interfaces,

TABLE 2. Bulk Domain Spacing of BrBCPs

group	sample codes	total degree of polymerization (DP)	L_o[a]
I	$[g\text{-}S_{2.4k}]_{19}$-b-$[g\text{-}LA_{2.4k}]_{25}$	44	19.2
	$[g\text{-}S_{2.4k}]_{35}$-b-$[g\text{-}LA_{2.4k}]_{43}$	78	33.6
	$[g\text{-}S_{2.4k}]_{51}$-b-$[g\text{-}LA_{2.4k}]_{67}$	118	54.6
	$[g\text{-}S_{2.4k}]_{98}$-b-$[g\text{-}LA_{2.4k}]_{124}$	222	91.0
	$[g\text{-}S_{2.4k}]_{189}$-$b$-$[g\text{-}LA_{2.4k}]_{233}$	422	157
	$[g\text{-}S_{2.4k}]_{259}$-$b$-$[g\text{-}LA_{2.4k}]_{381}$	640	*b*
II	$[g\text{-}S_{4.3k}]_{11}$-b-$[g\text{-}LA_{4.5k}]_{14}$	25	19.8
	$[g\text{-}S_{4.3k}]_{19}$-b-$[g\text{-}LA_{4.5k}]_{25}$	44	31.2
	$[g\text{-}S_{4.3k}]_{32}$-b-$[g\text{-}LA_{4.5k}]_{42}$	74	43.9
	$[g\text{-}S_{4.3k}]_{42}$-b-$[g\text{-}LA_{4.5k}]_{58}$	100	58.7
	$[g\text{-}S_{4.3k}]_{93}$-b-$[g\text{-}LA_{4.5k}]_{128}$	221	102.9
	$[g\text{-}S_{4.3k}]_{206}$-$b$-$[g\text{-}LA_{4.5k}]_{278}$	484	235[c]

[a] The domain spacing L_o is calculated from the corresponding first-order peak position of the 1-D SAXS profiles ($L_o = 2\pi/q^*$) unless noted. [b] Peaks are absent during the given experimental condition. [c] The first peak value is derived from the higher-order peaks.

using the local fractions of $\Phi_{AB}(\mathbf{r}_\perp) = \phi_A(\mathbf{r}_\perp) - \phi_B(\mathbf{r}_\perp)$, $\Phi_C(\mathbf{r}_\perp) = \phi_C(\mathbf{r}_\perp) - \langle\phi_C\rangle$, and $\Phi_e(\mathbf{r}_\perp) = \phi_e(\mathbf{r}_\perp) - \langle\phi_e\rangle$, where $\phi_\alpha(\mathbf{r}_\perp)$ is the volume fraction of α-segment at the position $\mathbf{r}_\perp$ along the direction perpendicular to the lamellar interface, $\langle\phi_\alpha\rangle$ is the average volume fraction of α-segment, and the subscript e stands for the end segment of backbone chain C. The three density profiles $\Phi_{AB}(\mathbf{r}_\perp)$, $\Phi_C(\mathbf{r}_\perp)$, and $\Phi_e(\mathbf{r}_\perp)$ for $N = 18$ and $M = 12$ were plotted as an example (Figure 6). It is noted from the density profiles that the distribution of backbone chain ends $\Phi_e(\mathbf{r}_\perp)$ are maximal in the midplane of lamellar phase, while the period in the profile of $\Phi_C(\mathbf{r}_\perp)$ is half that of $\Phi_{AB}(\mathbf{r}_\perp)$ with

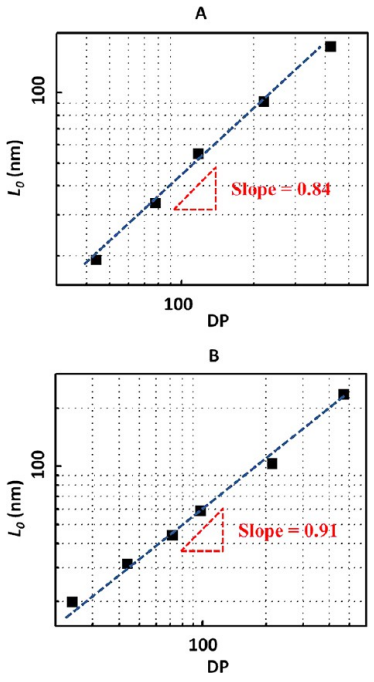

Figure 4. Scaling law between L_o and DP. (A) Group I. (B) Group II.

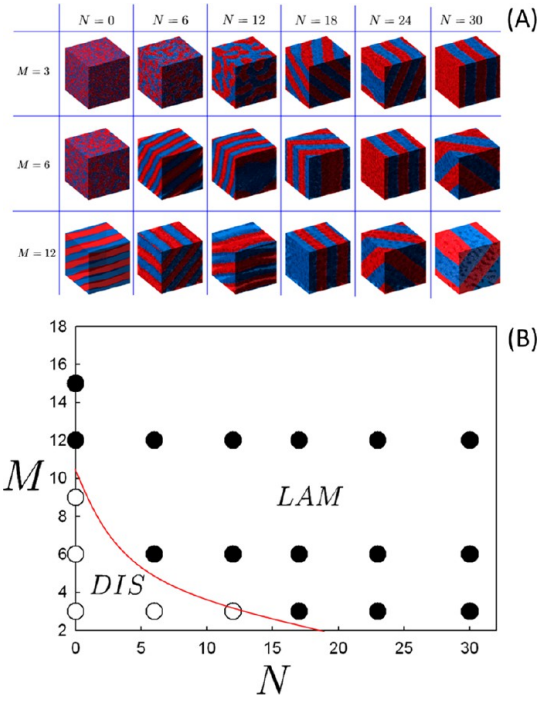

Figure 5. (A) Simulated morphologies of BrBCPs with a various set of variables (*N*,*M*). The regions of high density of A brush, B brush, and backbone (C) are colored blue, red, and black, respectively. (B) Phase map of molten BrBCP in the (*N*,*M*) space constructed from the simulation results. The filled circles represent the ordered lamellar phase (LAM), whereas the open circles denote the disordered state (DIS). The red line represents a guide to eye for the phase transition line from DIS to LAM.

small density depletion at the A/B interfaces. The other cases with ($N \neq 0$,M) show qualitatively similar profiles.

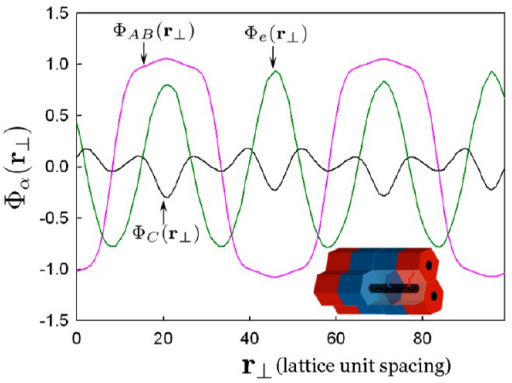

Figure 6. Local density difference between A and B brush (Φ_{AB}), local density of the backbone (Φ_C), and local density of the end segment of backbone chains (Φ_e) as a function of the position along the direction perpendicular to the lamellar interface for N = 18 and M = 12.

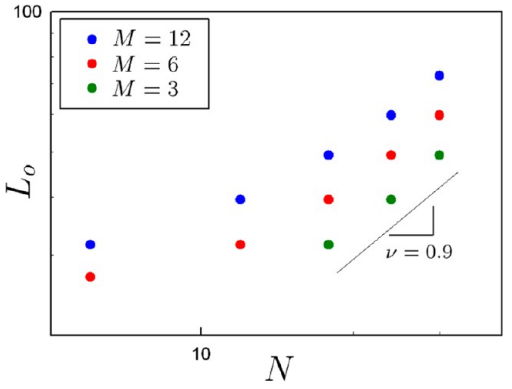

Figure 7. Interlamellar spacing L_o (in unit of lattice spacing) of the simulated BrBCP melt as a function of N for M = 12, 6, and 3.

This indicates that BrBCPs in the lamellae form bilayers with backbones orienting perpendicular to the A/B interface and with side chains orienting parallel to the A/B interface (see schematic in the inset of Figure 6).

Figure 7 shows the interlamellar spacing L_o as a function of backbone length N for different side chain length M. The interlamellar spacing was computed from the dominant scattering vector $\mathbf{q}^*$ in the scattering function defined by

$$S(q) = V^{-1} \sum_m \sum_n \langle \exp[i\mathbf{q}(\mathbf{r}_m - \mathbf{r}_n)] \Phi_{AB}(\mathbf{r}_m) \Phi_{AB}(\mathbf{r}_n) \rangle \quad (1)$$

where $\mathbf{q}$ is the scattering vector, V is the system volume, and $\Phi_{AB}(\mathbf{r}_m)$ is the volume fraction difference between A and B segment at position $\mathbf{r}_m$. The simulation results show that the exponent in the power from $L_o \sim N^\nu$ asymptotically approaches $\nu \cong 0.9$ as the backbone length N increases, in good agreement with the experimental result, suggesting that the backbones are stretched due to the steric force between side chains and due to the phase separation between A and B side chains that are grafted to the backbone in a blocky manner. The deviation from the power $\nu \cong 0.9$

for small N may be attributed to the weaker steric force. The steric effect from the brushes becomes reduced when a long backbone chain with many side chains is cut into some pieces of short backbones due to the significant backbone end effect where the steric effect vanishes. In addition, the weak degree of incompatibility is also responsible for the decrease of the exponent (recall that the system is disordered if $N \rightarrow 0$).

This near-linear dependence of the backbone length on the lamellar spacing can also be shown by a strong segregation theory.[17] Assuming that the molecular packing of BrBCPs in the unit cell of lamellar phase follows the geometry shown in Figure 8A, the total free energy (F) can be expressed in terms of interfacial and stretching energies, $F = F_{AB} + F_{AC} + F_{BC} + F_b + F_s$, where F_{AB}, F_{AC}, and F_{BC} are A/B, A/C, and B/C interfacial energies and F_b and F_s are the stretching energies of backbone and side chains, respectively. Considering the geometry of the unit cell (Figure 8A), each contribution of F (in unit of thermal energy k_BT) turns out to be

$$F_{AB} = \frac{\sqrt{6}\chi_{AB}^{1/2}R_c^2Na[M(3a - R_c) - R_c]}{3L_o(3a - R_c)} \quad (2)$$

$$F_{AC} = \frac{N}{3a - R_c}\left[\frac{R_c}{2}\chi_{AC} + \frac{\chi_{AC}^{1/2}a^2}{2\sqrt{6}R_c}(6 - a\rho_o R_c^2)\right] \quad (3)$$

$$F_{BC} = \frac{N}{3a - R_c}\left[\frac{R_c}{2}\chi_{BC} + \frac{\chi_{BC}^{1/2}a^2}{2\sqrt{6}R_c}(6 - a\rho_o R_c^2)\right] \quad (4)$$

$$F_b = \frac{\pi^2 L_o^2}{4Na^2} \quad (5)$$

$$F_s = \frac{3R_c}{2(3a - R_c)} + \frac{\pi^2 N(3R_s^4 - 8R_s^3R_c + 6R_s^2R_c^2 - R_s^4)}{16a^2(3Ma - MR_c - R_c)(R_s^2 - R_c^2)} \quad (6)$$

with a constraint for volume conservation

$$R_s = \left[\frac{(1 + M)(3a - R_c)R_c^2}{3a}\right]^{1/2} \quad (7)$$

where $\chi_{\alpha\beta}$ is the Flory interaction parameter between α and β segments, R_c is the radius of cylindrical domain formed by backbone C segments, a is the segment size, ρ_o is the mean segmental density, and R_s is a measure for the lateral size of unit cell relating to the center-to-center distance between cylindrical C domains L_c ($R_s/L_c = (\sqrt{3}/2\pi)^{1/2}$; see the schematic in Figure 8). Numerically minimizing the total free energy with respect to L_o and R_c gives the dependence of the lamellar spacing on the backbone length N and the side chain length M.

Figure 8 presents the theoretical results of interlamellar spacing L_o as a function of the backbone length N (Figure 8B) and the side chain length M (Figure 8C) for BrBCPs with the molecular parameters

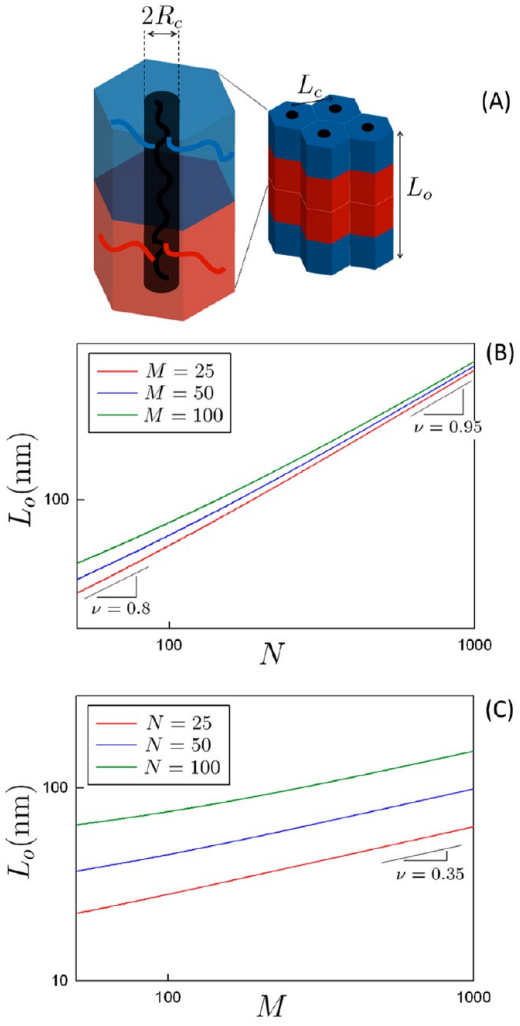

Figure 8. (A) Schematic of unit cell of lamellar phase formed by BrBCP. (B) Theoretical results for interlamellar spacing L_o as a function of N for M = 25, 50, and 100. (C) Theoretical results for interlamellar spacing L_o as a function of M for N = 25, 50, and 100.

of $\{a = 0.7\ \text{nm}, \rho_o = 6\ \text{nm}^{-3}, \chi_{AB} = 1.0, \chi_{AC} = 1.0, \chi_{BC} = 1.0\}$ where the degree of incompatibility (*i.e.*, $N\chi_{\alpha\beta}$ and $M\chi_{\alpha\beta}$) is large enough to validate the strong segregation approximation. The values of a and ρ_o are chosen as typical values in block copolymer melt. As shown in Figure 8B and 8C, it is found from strong segregation theory that the dependence of the interlamellar spacing asymptotically approaches $L_o \sim N^{0.95}$ (N is equivalent to DP in Figure 4) for large N and $L_o \sim M^{0.35}$ for large M, which is in good agreement with both experimental and simulation results.

Fast Kinetics of Self-Assembly in the Bulk. Polymer entanglement causes a kinetic barrier for polymers to self-assemble, thus leading to a slow kinetic process of the self-assembly. As the polymers grow bigger, entanglement can have increased effect on the self-assembly process. The typical value of the entanglement molecular weight M_e, above which the self-diffusion constant D of the chain molecules is changed from $D \sim N^{-1}$

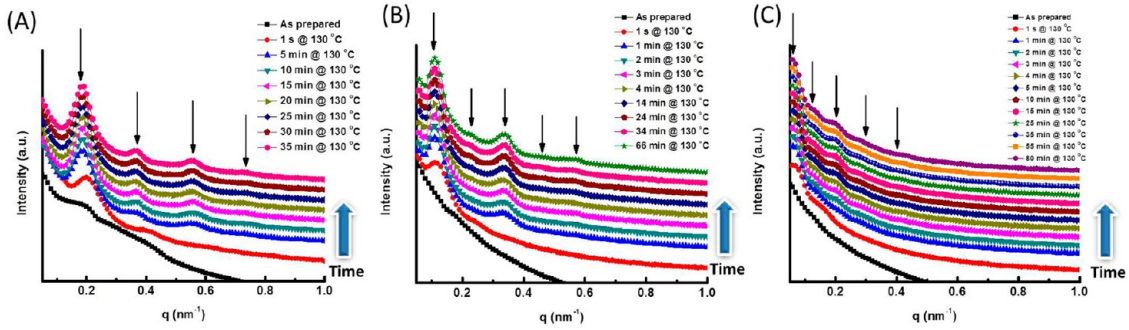

Figure 9. *In situ* SAXS of sample (A) $[g\text{-}S_{2.4k}]_{35}$-*b*-$[g\text{-}LA_{2.4k}]_{43}$, (B) $[g\text{-}S_{2.4k}]_{51}$-*b*-$[g\text{-}LA_{2.4k}]_{67}$, and (C) $[g\text{-}S_{2.4k}]_{98}$-*b*-$[g\text{-}LA_{2.4k}]_{124}$.

(non-entangled, Rouse dynamics) to $D \sim N^{-2.4}$, is on the order (O) of O(1) ~ O(10) kDa. Brush polymers have, on the other hand, been reported to show non-entangled dynamics at the high MW regime up to several thousand kilodaltons,[18] which allows us to expect a more rapid self-assembly process even for the ultra-high MW (hundreds to thousands of kilodaltons as indicated in Table 1) of BrBCPs. This inspired us to take a closer look at the unique properties of those BrBCPs and their self-assembly behavior in the bulk state. *In situ* SAXS was used to monitor the kinetics of the self-assembly process. Figure 9 shows representative examples of samples $[g\text{-}S_{2.4k}]_{35}$-*b*-$[g\text{-}LA_{2.4k}]_{43}$, $[g\text{-}S_{2.4k}]_{51}$-*b*-$[g\text{-}LA_{2.4k}]_{67}$, and $[g\text{-}S_{2.4k}]_{98}$-*b*-$[g\text{-}LA_{2.4k}]_{124}$. For instance, in Figure 9B, the initial state as indicated by the bottom black curve did not show any distinct peak and exhibited a gradual decrease in intensity, suggesting that chains of BrBCPs were in random arrangements. A measurement was taken immediately (1 s, red curve) once the temperature was increased to 130 °C and a primary peak at ~0.012 $Å^{-1}$ appeared. This implies that a characteristic distance was developed, although not too well-defined due to its broad shape. Upon longer annealing time, the primary scattering wavevector q^* shifted a little bit to smaller q value (0.011 $Å^{-1}$) and higher-order reflections were profoundly enhanced at integral multiples of q^*, an evidence of improvement in lateral order of lamellar structures. Notably, low MW BrBCP (Figure 9A) self-assembled much more rapidly (~5 min) in comparison to the high MW (Figure 9C, ~1 h). It is understandable that low MW BrBCP has less entanglement between chains and thus the mobility is higher. Nevertheless, these results show that well-ordered lamellar structures were formed within an hour for all of the samples shown. As a comparison, we also tried *ex situ* SAXS experiments with the largest MW of a linear lamellar forming PS-*b*-PLA BCP that we have (Polymer Source, 21k-*b*-24.3k, PDI = 1.14). We found that, even after thermal annealing for 24 h at 130 °C, the order was not well-developed (Supporting Information, Figure S3). This reflects the advantage of a BrBCP for its rapid kinetics on the other side.

CONCLUSION

In summary, symmetric BrBCPs of PLA and PS side chains self-assemble rapidly into highly ordered lamellar domains ranging from 20 to 240 nm as revealed by SAXS. The domain size increased approximately linearly with the MW of the backbone, which indicated that the backbone was in an extremely extended conformation. Strong segregation theory and Monte Carlo simulation of ordered BrBCPs revealed that the direction of backbones is perpendicular to the interface between lamellar domains formed by PS and PLA brushes that are oriented parallel to the interface in the lamellar structure, which is essentially different from the molecular packing in linear diblock lamellae. This molecular packing is responsible for the near-linear dependence of the domain spacing on backbone length, rationalizing experimental results. Those BrBCPs provide an ideal model system to study the self-assembly of other BrBCPs and may enlighten structure designing of BCPs that are capable of fast self-assembly into nanostructures with a wide range of domain spacing.

EXPERIMENTAL SECTION

Small-Angle X-ray Scattering (SAXS). We investigated the self-assembly of BrBCPs in the bulk state using small-angle X-ray scattering (SAXS). Since T_g of PS was determined to be around 95 °C and T_g of PLA in the BrBCP was found to be around 50 °C (Supporting Information, Figure S2), an elevated temperature of 130 °C was chosen to perform the thermal annealing experiments of those BrBCPs. The solid samples were pressed in aluminum washers which are windowed by Kapton films and kept in vacuum oven for 12 h or longer to achieve thermal equilibrium. SAXS measurements for group I BrBCPs were performed at beamline 7.3.3 at the Advanced Light Source, Berkeley National Laboratory (Figure 1). The wavelength of incident X-ray was 0.124 nm. The sample-to-detector distance was 3889.2 mm. Scattering signals were collected by a Pilatus 100k fast detector with pixel size of 0.172 mm. SAXS measurements for group II BrBCPs were performed at beamline X27C, National Synchrotron Light Source, Brookhaven National Laboratory. The wavelength of incident X-ray was 0.1371 nm. The sample-to-detector distance was 1786.5 mm. A marCCD detector with pixel size of 0.158 mm was used to collect the scattering signals. For both beamlines, the exposure time was kept between 30 and 60 s.

***In Situ* Small-Angle X-ray Scattering.** *In situ* SAXS measurements were performed at beamline 8-ID-E, Advanced Photon Source, Argonne National Laboratory. The wavelength of incident X-ray was 0.1687 nm. The sample-to-detector distance was 1641.0 mm.

The samples were mounted onto an Instec HCS410 hot stage equipped with liquid nitrogen cooling and nitrogen gas purging accessories. The temperature was programed to increase fast from room temperature to 130 °C at a rate of 50 °C/min and held at that temperature. The exposure time for each snapshot was limited to 0.5−1 s in order to minimize the damage to the samples that can be probably caused by the X-ray photons.

Simulations. Dynamic Metropolis Monte Carlo method with the 8-site bond fluctuation model[15,16] was used. For the simulation of the bulk morphology of BrBCPs, bead spring chains of BrBCP chains, each with N backbone beads of type C to which equal numbers of A and B side chains with M beads each, were sequentially grafted and were generated on a cubic box with $L \times L \times L$ under periodic boundary conditions. The system was then equilibrated with the set of interaction parameters of $\varepsilon = \varepsilon_{AB} = \varepsilon_{BC}/2 = \varepsilon_{AC}/2 = 0.4\ k_BT$, where the segmental interaction parameters $\varepsilon_{\alpha\beta}$ between the components α and β were given considering the solubility parameters of the PS, PLA, and polynorbornene.[19,20] The number of segments of backbone N and the number of segments of side chain M are varied from $N = 6$ to $N = 30$ and from $M = 3$ to $M = 12$. For comparison, the case of $N = 0$, which corresponds to a symmetric diblock copolymer with chain length $2M$, was also simulated. A lattice occupation density is set to be $\phi = 0.5$ for polymer chains in the simulation box, which corresponds to a polymer melt in the bond fluctuation model.[21] Starting from a random initial configuration, the film system is allowed to equilibrate for 5×10^7 Monte Carlo steps (MCS). Configurations sampled at every 10^4 MCS after equilibration and the mean local densities of the simulation components were obtained by averaging the densities over 100 samples.

Conflict of Interest: The authors declare no competing financial interest.

Acknowledgment. This work was supported by the Department of Energy Office of Basic Energy Science under Contract Nos. DE-FG02-96ER45612 and DE-FG02-04ER46126 and the NSF-supported Materials Research Science and Engineering Center at UMass. Authors acknowledge the use of the Advanced Light Source, Berkeley National Laboratory, which was supported by the Director, Office of Science, Office of Basic Energy Sciences, of the U.S. Department of Energy under Contract No. DE-AC02-05CH11231; use of the National Synchrotron Light Source, Brookhaven National Laboratory, which was supported by the U.S. Department of Energy, Office of Science, Office of Basic Energy Sciences, under Contract No. DEAC02-98CH10886; use of the Advanced Photon Source, an Office of Science User Facility operated for the U.S. Department of Energy (DOE) Office of Science by Argonne National Laboratory, which was supported by the U.S. DOE under Contract No. DE-AC02-06CH11357. J. Huh acknowledges the supports from Samsung Display, Korea.

Supporting Information Available: GPC and DSC of group I and group II BrBCPs, SAXS of linear PS-*b*-PLA (21k-*b*-24.3k) are available. This material is available free of charge *via* the Internet at http://pubs.acs.org.

REFERENCES AND NOTES

1. Bates, F. S.; Fredrickson, G. H. Block Copolymer Thermodynamics: Theory and Experiment. *Annu. Rev. Phys. Chem.* **1990**, *41*, 525–557.
2. Hamley, I. W. *The Physics of Block Copolymers*; Oxford University Press: New York, 1998.
3. Segalman, R. A. Patterning with Block Copolymer Thin Tilms. *Mater. Sci. Eng. R* **2005**, *48*, 191–226.
4. Tsui, O. K. C.; Russell, T. P. *Polymer Thin Films*; World Scientific: Singapore, 2008.
5. Fredrickson, G. H.; Bates, F. S. Dynamics of Block Copolymers: Theory and Experiment. *Annu. Rev. Mater. Sci.* **1996**, *26*, 501–550.
6. Park, S.; Lee, D. H.; Xu, J.; Kim, B.; Hong, S. W.; Jeong, U.; Xu, T.; Russell, T. P. Macroscopic 10-Terabit-per-Square-Inch Arrays from Block Copolymers with Lateral Order. *Science* **2009**, *323*, 1030–1033.
7. Cushen, J. D.; Otsuka, I.; Bates, C. M.; Halila, S.; Fort, S.; Rochas, C.; Easley, J. A.; Rausch, E. L.; Thio, A.; Borsali, R.; *et al.* Oligosaccharide/Silicon-Containing Block Copolymers with 5 nm Features for Lithographic Applications. *ACS Nano* **2012**, *6*, 3424–3433.
8. Kang, Y.; Walish, J. J.; Gorishnyy, T.; Thomas, E. L. Broad-Wavelength-Range Chemically Tunable Block-Copolymer Photonic Gels. *Nat. Mater.* **2007**, *6*, 957–960.
9. Miyake, G. M.; Weitekamp, R. A.; Piunova, V. A.; Grubbs, R. H. Synthesis of Isocyanate-Based Brush Block Copolymers and Their Rapid Self-Assembly to Infrared-Reflecting Photonic Crystals. *J. Am. Chem. Soc.* **2012**, *134*, 14249–14254.
10. Leibler, L. Theory of Microphase Separation in Block Copolymers. *Macromolecules* **1980**, *13*, 1602–1617.
11. Runge, M. B.; Bowden, N. B. Synthesis of High Molecular Weight Comb Block Copolymers and Their Assembly into Ordered Morphologies in the Solid State. *J. Am. Chem. Soc.* **2007**, *129*, 10551–10560.
12. Xia, Y.; Olsen, B. D.; Kornfield, J. A.; Grubbs, R. H. Efficient Synthesis of Narrowly Dispersed Brush Copolymers and Study of Their Assemblies: The Importance of Side Chain Arrangement. *J. Am. Chem. Soc.* **2009**, *131*, 18525–18532.
13. Oono, Y.; Bahiana, M. $^2/_3$-Power Law for Copolymer Lamellar Thickness Implies a $^1/_3$-Power Law for Spinodal Decomposition. *Phys. Rev. Lett.* **1988**, *61*, 1109–1111.
14. Zalusky, A. S.; Olayo-Valles, R.; Wolf, J. H.; Hillmyer, M. A. Ordered Nanoporous Polymers from Polystyrene-Polylactide Block Copolymers. *J. Am. Chem. Soc.* **2002**, *124*, 12761–12773.
15. Carmesin, I.; Kremer, K. Static and Dynamic Properties of Two-Dimensional Polymer Melts. *J. Phys. (Paris)* **1990**, *51*, 915–932.
16. Deutsch, H. P; Binder, K. Interdiffusion and Self-Diffusion in Polymer Mixtures: A Monte Carlo Study. *J. Chem. Phys.* **1991**, *94*, 2294–2304.
17. Grason, G. M. The Packing of Soft Materials: Molecular Asymmetry, Geometric Frustration and Optimal Lattices in Block Copolymer Melts. *Phys. Rep.* **2006**, *433*, 1–64.
18. Hu, M.; Xia, Y.; McKenna, G. B.; Kornfield, J. A.; Grubbs, R. H. Linear Rheological Response of a Series of Densely Branched Brush Polymers. *Macromolecules* **2011**, *44*, 6935–6943.
19. Vayer, M.; Hillmyer, M. A.; Dirany, M.; Thevenin, G.; Erre, R.; Sintrurel, C. Perpendicular Orientation of Cylindrical Domains upon Solvent Annealing Thin Films of Polystyrene-*b*-Polylactide. *Thin Solid Films* **2010**, *518*, 3710–3715.
20. Li, Z.-H.; Ying, X.-G.; Liu, G. J. The Internal Pressure and New Solubility Parameter of Polymeric Liquids. *J. Chem. Eng.* **2001**, *15*, 206–212.
21. Thompson, R. L.; McDonald, M. T.; Lenthall, J. T.; Hutchings, L. R. Solvent Accelerated Polymer Diffusion in Thin Films. *Macromolecules* **2005**, *38*, 4339–4344.
22. Sveinbjörnsson, B. R.; Weitekamp, R. A.; Miyake, G. M.; Xia, Y.; Atwater, H. A.; Grubbs, R. H. Rapid Self-Assembly of Brush Block Copolymers to Photonic Crystals. *Proc. Natl. Acad. Sci. U.S.A.* **2012**, *109*, 14332–14336.
23. Poelma, J. E.; Ono, K.; Miyajima, D.; Aida, T.; Satoh, K.; Hawker, C. J. Cyclic Block Copolymers for Controlling Feature Sizes in Block Copolymer Lithography. *ACS Nano* **2012**, *6*, 10845–10854.
24. Hawker, C. J.; Russell, T. P. Block Copolymer Lithography: Merging "Bottom-Up" with "Top-Down" Processes. *MRS Bull.* **2005**, *30*, 952–966.
25. Bang, J.; Jeong, U.; Ryu, D. Y.; Russell, T. P.; Hawker, C. J. Block Copolymer Nanolithography: Translation of Molecular Level Control to Nanoscale Patterns. *Adv. Mater.* **2009**, *21*, 4769–4792.